

# Multi-objective vibro-acoustic optimization of stiffened panels

Pankaj Joshi · Sameer B. Mulani · Rakesh K. Kapania

Received: 6 February 2014 / Revised: 10 August 2014 / Accepted: 28 August 2014 / Published online: 30 October 2014  
© Springer-Verlag Berlin Heidelberg 2014

**Abstract** A multi-objective vibro-acoustic design optimization of straight or curvilinearly stiffened panels excited by an acoustic diffuse field is performed. During design optimization, the panel mass and the radiated acoustic power are the two objectives to be minimized while satisfying constraints on buckling, von Mises stress and crippling. Based on the concept of plane wave propagation, a diffuse acoustic field is developed for use along with a finite element model. To represent the panel's structural behavior, the dynamic analysis of the panel is performed for the developed diffuse acoustic excitation and the radiated acoustic power is calculated using the velocities obtained from the dynamic analysis. A baseline design is obtained by optimization study with mass as an objective to be minimized while constraints are put on buckling, von Mises stress and crippling. The obtained baseline grid stiffened panel is

used for a comparative study of a panel with curvilinear stiffeners in vibro-acoustics with diffuse sound field as the source of the excitation.

**Keywords** Turbulent boundary layer · Sound power · Curvilinear stiffener · Power spectral density · Pareto optimal designs

## Nomenclature

$M$	Mass Matrix
$K$	Stiffness Matrix
$C$	Damping Matrix
$F$	External Dynamic Force, $N$
$m$	Mass, kg
$p$	Pressure at the data recovery point, $N/m^2$
$v_n$	Surface normal velocity of the plate, $m/s$
$a$	Length of the plate, $m$
$b$	Width of the plate, $m$
$W$	Radiated acoustic power, $Watt$

---

P. Joshi (✉)  
Virginia Polytechnic Institute and State University,  
Blacksburg, VA 24060, USA  
e-mail: pjoshi81@vt.edu

S. B. Mulani  
Department of Aerospace and Ocean Engineering, Virginia  
Polytechnic Institute and State University, 460 Old Turner St.,  
Blacksburg, VA 24060, USA

R. K. Kapania  
Department of Aerospace and Ocean Engineering, Virginia  
Polytechnic Institute and State University, Blacksburg, VA 24060,  
USA

*Present Address:*  
P. Joshi  
Heinkel Engineering GmbH Co. KG, Hamburg, Germany

S. B. Mulani  
Department of Aerospace Engineering and Mechanics, University  
of Alabama, Tuscaloosa, AL 35487, USA

## 1 Introduction

The noise regulations around the world have increased the need to design aircraft panels to have reduced sound radiation (Graham 1996a, 1996b). In the past, the designers used to design an aircraft panel for structural performance only and then an acoustic treatment was employed to reduce the sound radiation characteristics of these panels. The new trend is to design an aircraft panel having a reduced sound radiation performance during the design stage itself (Koopmann and Fahnline 1997). This approach of designing panels for reduced sound radiation at the design stage itself, makes the whole design process more complex as the designer needs to know the

trade-off between the mass of the structure and the vibro-acoustic performance.

Minimizing acoustic response of a structure can be done using two approaches (Denli et al. 2005). In the first approach, response of a structure to the excitation is calculated and then the acoustic power radiated from the structure is obtained. Now, optimization is done by changing the design parameters. The second approach decouples the acoustic and structural domains. In the second approach the surface velocity profile of the structure for minimum acoustic response is found first and then the design parameters are calculated to meet the desired velocity profile. Optimal structural design problems to reduce sound radiation are computationally expensive and highly nonlinear in design variables and acoustic response; even most of the conventional methods such as gradient based design optimization, are difficult to apply. Jeon and Okuma (2004) used a particle swarm optimization (PSO) algorithm for optimal bending design of a vibrating plate to minimize noise radiation.

Belegundu, (Salagame and Koopmann 1994) designed a baffled plate excited by single frequency and broadband harmonic excitation to minimize the radiated acoustic power using a gradient-based optimization algorithm. Lu-yun and De-yu (2007) used the finite element method (FEM) to obtain structural frequency response, the boundary element method (BEM) for low frequency acoustic radiation, and genetic algorithm (GA) for structural-acoustic optimization. In the work done by Lu-yun and De-yu (2007), the authors assumed that the structural and the acoustic responses are uncoupled. Fourie and Groenwold (2002) presented an application of PSO algorithm to the optimal shape and size design with respect to static load. Fourie and Groenwold (2002) reported that PSO yielded better solutions than GAs for geometry optimization of simple truss structures.

St. Pierre and Koopmann (1993) used a more direct optimization process resulting in surface velocity profiles having the same characteristic as the weak radiators (Koopmann and Fahnline 1997). (Cunefare 1990, Naghshineh 1992; St. Pierre and Koopmann 1993) reported that the radiated acoustic power reduction can be accomplished by surface velocity redistribution such that adjacent areas of high and low acoustic pressure on the boundary surface balance each other. A single area of balanced high and low acoustic pressure radiates sound as a dipole source (Pierce 1989) while an area of unbalanced high and low acoustic pressure radiates more like a monopole (Pierce 1989). Thus changing radiation from a collection of monopole sources to a collection of dipole sources can bring a large change in power output.

Hekamati, Ricot, and Druault (2010) studied the vibro-acoustic behavior of plate excited by aero-acoustic pressure field and used the combination of turbulent boundary layer (TBL) pressure and acoustic diffuse field as the source

of excitation. They found that the radiated acoustic (pressure) field associated to the diffuse field excitation is almost 10 dB higher than the TBL excitation. In a similar study, (Maury, Gardonio and Elliott 2002) used the wavenumber approach to study the vibro-acoustics of the plate. Maury, Gardonio and Elliott (2002) observed that the modes that contribute to the panel response under a diffuse field excitation are more efficiently excited than in the case of TBL excitation. They also concluded that the levels for the vibration response (radiated acoustic power) of the panel excited by diffuse field are higher by up to 20–25 dB than those observed for TBL excitation. In a previous work, (Joshi et al. 2010a) have designed a stiffened panel with point excitation only. Later on the authors also extended this work and developed a framework (Joshi et al. 2010b) to design panels with curvilinear stiffeners subjected to turbulent boundary layer excitation. It was observed that it is very expensive and hard to simulate the TBL excitation in a test environment while diffuse field can be simulated with relatively less cost and effort. The diffuse field is the simplest way to simulate an excitation in an acoustic environment such as the shuttle launch (Faust and Piret 1996). Moreover, to the best of authors' knowledge, the design optimization study of a panel with curvilinear stiffeners under diffuse field excitation has not been addressed in the literature. Therefore, in this paper we perform design optimization of stiffened panels excited by a diffuse acoustic field.

The diffuse acoustic field is generated following the approach suggested by Buehrle et al. (2003) The objectives of this design optimization study are to reduce the mass and the sound radiation due to vibro-acoustic phenomena while meeting all the structural requirement such as buckling, von Mises stress and crippling stress in the structure. Due to conflicting nature of objectives, non dominated sorting genetic algorithm-II (NSGA-II) (Deb et al. 2002) in VisualDOC 6.2.2 (2010) is used to perform the multi-objective design optimization using the developed framework (Joshi et al. 2010a, b, Mulani et al. 2013), termed as *EBF3PanelOpt*, for the diffuse field excitation. The work in the rest of the paper is discussed in six sections. Following the introduction, Section 2 explains the approach for the construction of diffuse field excitation. Section 3 discusses the vibro-acoustic response calculation for the used diffuse field excitation. Section 4 deals with structural-acoustic optimization problem formulation. Results are discussed in Section 5 followed by a section on conclusions and future work in Section 6.

## 2 Construction of diffuse acoustic field

To capture the effect of the diffuse field excitation, a large number,  $N$ , of plane waves with random angles of incidence,

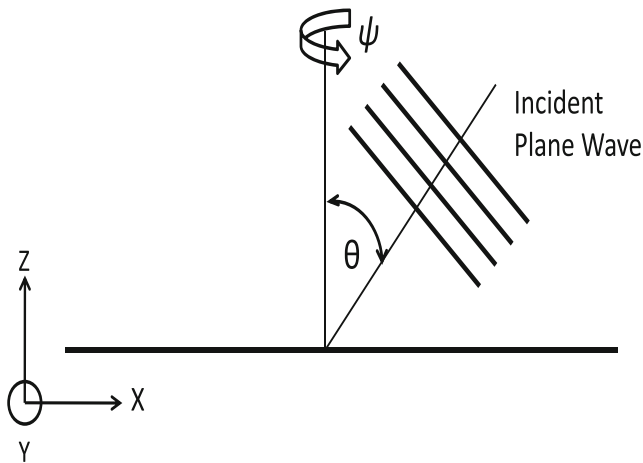


**Fig. 1** The plane wave propagating in the x-z plane and incident at angles  $\theta$  and  $\psi$  on the stiffened panel

random magnitude and random temporal phase angles were summed. A similar approach is used by Buehrle et al. (2003). The plane wave, incident on a panel at angles  $\theta_q$  and  $\psi_q$ , is shown in Fig. 1. The angles  $\theta_q$  and  $\psi_q$  are uniformly distributed random numbers on the intervals  $[-\pi/2, \pi/2]$  and  $[0, 2\pi]$  respectively and represent the angles of propagation in spherical coordinates. The  $q^{th}$  plane wave has a magnitude of  $P_q \cos(\theta_q)$ , where  $P_q$  is a uniformly distributed random number in the interval  $[0,1]$ . With this analogy, the pressure due to a single plane wave is given as:

$$P_q(x, y, z; t) = P_q \cos(\theta_q) e^{-i(k_x x + k_y y + k_z z)} e^{i(\omega t + \beta_q)} \quad (1)$$

Where  $\omega$  is the angular frequency,  $k$  is the ratio of the angular frequency and the speed of sound in the acoustic medium,  $\beta_q$  is a random temporal phase angle uniformly distributed on the interval of  $[0, 2\pi]$ ; and  $k_x, k_y$  and  $k_z$  are the wavenumber in the x, y and z directions, respectively, and can be written as:

$$k_x = k \sin(\theta_q) \cos(\psi_q) \quad (2)$$

$$k_y = k \sin(\theta_q) \sin(\psi_q) \quad (3)$$

$$k_z = k \cos(\theta_q) \quad (4)$$

Assuming a steady state simple harmonic motion, and furthermore a rigid boundary condition at the interface between the panel and the acoustic medium, the spatial distribution of the sound field pressure exciting the panel is given as:

$$\bar{P}_q(x, y, z; \omega) = 2P_q \cos(\theta_q) e^{-i(k_x x + k_y y + k_z z - \beta_q)} \quad (5)$$

The total pressure at the centroid of the element,  $P_e$ , due to  $N$  incident plane waves, can be given as:

$$P_e(x, y, z; \omega) = \sum_{q=1}^N 2P_q \cos(\theta_q) e^{-i(k_x x + k_y y + k_z z - \beta_q)} \quad (6)$$

In a similar work to construct the diffuse field, (Rafaely 2000) used the value of  $N$  to be 1145. Due to large number of frequencies, any value of  $N$  which is higher than 1000 created memory problem in generating the acoustic diffuse field. Therefore, for the research work in this paper, the value of  $N$  is assumed to be 1000. The total pressure at the centroid of each element in a finite element model is calculated using (6). A coarse finite element model is used for the calculation of the acoustic diffuse field at the centroid of each element. A coarse mesh is used to make the design optimization task affordable from CPU time point of view for each analysis. Once the diffuse field is generated, the design optimization study is performed using this diffuse field as the source of excitation.

For every velocity response calculation during the optimization, the generated pressure field at the centroid of each element of the coarse mesh is applied to the elements of the refined mesh of the stiffened panel using PLOAD4 card in MD NASTRAN. The velocity response due to this pressure excitation is calculated for a frequency range from 20 Hz to 1000 Hz with a step size of 5 Hz. This velocity data is then used to calculate the radiated acoustic power from the stiffened panel.

### 3 Vibro-acoustic response calculation

The structural vibration response analysis is the basis of structural-acoustic optimization. In the present work, the structural-acoustic optimization is carried out using a philosophy called noise-control-by-design (Constans et al. 1998) wherein the radiated sound from a vibrating structure is treated as an objective during structural-acoustic design optimization study. The aim of this design philosophy is to reduce the noise generated by the structure by changing the structural design itself. To achieve this goal, optimization techniques are used and an optimal design is obtained. During the optimization process, structural and acoustic responses are calculated and sent to the optimizer and the optimizer generates next set of design points such that there is an improvement in both, the structural and the acoustic responses. Structural and acoustic response calculations are discussed in following subsections.

#### 3.1 Structural response

The equation of motion for a multi-dimensional vibrating structure,  $\Omega^S$  under a dynamic load,  $F(t)$ , if fluid medium influence is not considered, can be represented as:

$$\mathbf{M}\ddot{\mathbf{U}} + \mathbf{C}\dot{\mathbf{U}} + \mathbf{K}\mathbf{U} = \mathbf{F}(t), \quad t > 0. \quad (7)$$

Where  $\mathbf{U}$  is the nodal displacement vector,  $\mathbf{M}$  is the structural mass matrix,  $\mathbf{C}$  is the viscous damping matrix, and  $\mathbf{K}$  is the structural stiffness matrix. If we assume a harmonic excitation,  $\mathbf{F}(t)$  can be expressed as:

$$\mathbf{F}(t) = \mathbf{f}(\omega)e^{i\omega t} \tag{8}$$

Where  $f(\omega)$  is the magnitude of the harmonic load,  $\omega$  is the frequency of excitation,  $i$  is the imaginary number ( $i^2 = -1$ ). The nodal displacement vector can be expressed as  $\mathbf{U}(t) = \mathbf{u}(\omega)e^{i\omega t}$ , where  $\mathbf{u}(\omega)$  is the nodal complex displacement vectors. Time dependency of the dynamic problem can be eliminated using  $\mathbf{U}(t) = \mathbf{u}(\omega)e^{i\omega t}$  as the displacement vector and (8) as a harmonic excitation. The frequency response equation, thus obtained, can be written as:

$$\left\{ -\omega^2\mathbf{M} + i\omega\mathbf{C} + \mathbf{K} \right\} \mathbf{u}(\omega) = \mathbf{f}(\omega) \tag{9}$$

In shorthand, frequency response equation can be expressed as:  $\mathbf{A}(\omega)\mathbf{u}(\omega) = \mathbf{f}(\omega)$ . Where,  $\mathbf{A}(\omega) = -\omega^2\mathbf{M} + i\omega\mathbf{C} + \mathbf{K}$ . Using (9), the nodal displacement vector matrix is written as:

$$\mathbf{u}(\omega) = \mathbf{A}(\omega)^{-1}\mathbf{f}(\omega) \tag{10}$$

Using displacement vector, the velocity vector  $\mathbf{v}(\omega)$  can be expressed as  $\mathbf{v}(\omega) = i\omega\mathbf{u}(\omega)$ . At the interface between the structure and the fluid, with the assumption that the structure and the fluid are uncoupled, the nodal particle normal velocity vector can be written as:

$$\mathbf{v}_n(\omega) = i\omega\mathbf{T}\mathbf{A}(\omega)^{-1}\mathbf{f}(\omega) \tag{11}$$

In (11),  $\mathbf{T}$  is a transformation matrix which converts the velocity vector to a velocity vector normal to the surface of the structure. MD NASTRAN (1999) is used to calculate the nodal velocities as the response quantity of interest to the applied diffuse field excitation for a range of frequencies from 20 Hz to 1000 Hz in a step of 5 Hz. The diffuse field pressure excitation is given by (6) in the Section 2 and applied to the elements in the finite element model. The nodal particle normal velocity is obtained using nodal velocity and used as the input for acoustic response calculation.

### 3.2 Acoustic response

The pressure radiated to a point in the acoustic medium from a planar structure can be written solely in terms of the normal vibration of the radiating surface and it is calculated using the following well-known Rayleigh integral (Wallace 1972)

$$p(\bar{r}) = \frac{j\omega\rho_0}{2\pi} e^{j\omega t} \int_S \frac{v_n(\bar{r}_s)e^{-jk|\bar{r}-\bar{r}_s|}}{|\bar{r}-\bar{r}_s|} dS \tag{12}$$

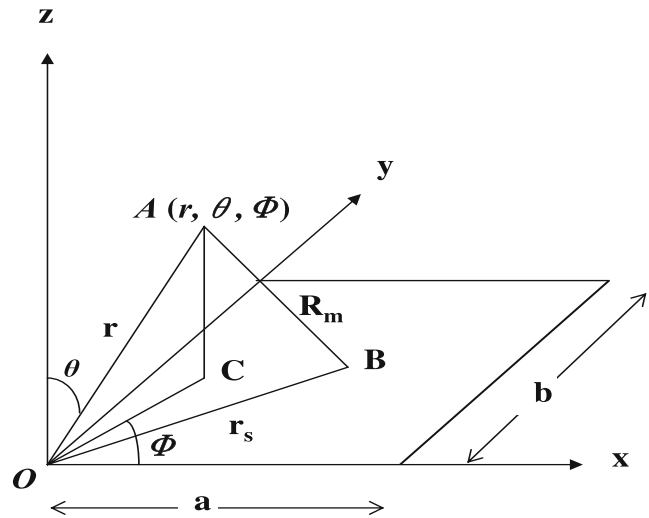


Fig. 2 Simply supported rectangular panel on the x-y plane with the origin at O

Where,  $\bar{r}$  is the position vector of the point at which the pressure is being determined and  $\bar{r}_s$  is the position vector locating a surface element of the vibrating structure as shown in the Fig. 2 (Fahy 1985),  $A$  is the observation point in far field,  $B$  is the location of elemental noise source (simple source),  $a$  and  $b$  are the length and the width of the panel, respectively; and  $r, \theta,$  and  $\phi$  are spherical co-ordinate centered at the origin  $O$ . The pressure is calculated using Rayleigh integral as shown in (12).

The vibrational results are obtained by the FEM. From a FEM representation of a vibrating structure, the velocity of the structure at a number of defined nodal locations is known. Combining the nodal velocities with the knowledge of the structure’s geometry, the normal surface velocity may be computed for each element comprising the structure. This discretized normal surface velocity suggests that Rayleigh integral can be calculated numerically by a summation over the elements comprising the complex structure. This discretization takes the following form:

$$p(\bar{r}) = \sum_{m=1}^{N_{ele}} \frac{j\omega\rho_0}{2\pi} A_m v_m \frac{e^{-jkR_m}}{R_m} \tag{13}$$

where the index  $m$  identifies an element of the vibrating structure,  $N_{ele}$  is the total number of elements,  $A_m$  is the area of the  $m^{th}$  element,  $v_m$  is the normal velocity of the  $m^{th}$  element, and  $R_m$  is the distance between the center of the  $m^{th}$  element and the point in acoustic medium at which the pressure is to be evaluated. Normal velocity,  $v_m$  is calculated by taking the dot product of average elemental velocity at the centroid and the unit normal vector for the element under consideration. Average elemental velocity at the centroid of the element is calculated by averaging nodal velocities obtained using

triangular element (CTRIA3) in MD NASTRAN (1999). Now, the radiated time average acoustic power ( $W$ ) can be calculated by summing the product of the radiated intensity (Fahy 1985) at the centroid of an element and the area of the corresponding element on a hemisphere enclosing the vibrating structure. The radius of the hemisphere is ten times the largest dimension of the vibrating structure. Numerically, the radiated sound power can be calculated as:

$$W = \sum_{i=1}^{N_\theta} \sum_{j=1}^{N_\phi} \frac{|p(r, \tilde{\theta}_i, \tilde{\phi}_j)|^2}{2\rho c} r^2 \sin(\tilde{\theta}_i) \delta\theta \delta\phi \quad (14)$$

where,

$$\delta\theta = \frac{\pi}{2N_\theta}; \delta\phi = \frac{2\pi}{N_\phi}; \tilde{\theta}_i = i\delta\theta; \tilde{\phi}_j = j\delta\phi \quad (15)$$

All of the information necessary for implementation of this approach is readily extracted from the FEM model. This method is most appropriately applied to planar, baffled radiators. In the present work, we have used Rayleigh integral approach to calculate the acoustic pressure.

### 4 Optimization problem formulation

#### 4.1 Problem definition

For the optimization problem in this paper, the velocity response of a structure to the excitation is calculated first, and then the acoustic power radiated from the structure is obtained. Now, optimization is done by changing the design parameters such that the radiated power from the structure

is minimized. In general, mathematically we can define the optimization problem as follows.

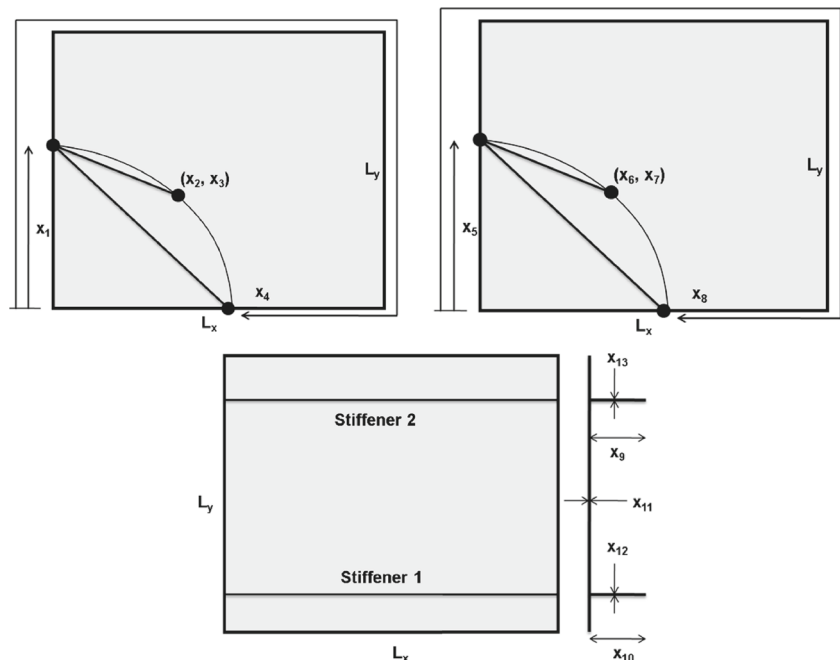
$$\begin{aligned} \min_{\mathbf{x}} \quad & f_0(\mathbf{x}) \\ & f_i(\mathbf{x}) \leq 1, \quad i = 1, \dots, N_{cons} \\ & A_j \leq \mathbf{x}_j \leq B_j, \quad j = 1, \dots, N_{dvar} \end{aligned} \quad (16)$$

As given in (16),  $f_0$  is the objective function that has to be minimized with respect to design variables  $\mathbf{x}$ , while satisfying the constraints  $f_i$  shown in (16). In (16),  $N_{cons}$  is the total number of constraint and  $N_{dvar}$  is the number of design variables in the optimization problem at hand. The design variables indicated by vector  $x$  are subjected to constraints (often called as side constraints) in the form of upper limits ( $B_j$ ) and lower limits ( $A_j$ ). These are expressed in (16). Mathematical correlation to the optimization problem is explained in the following subsections.

#### 4.2 Design variables

The response of a structure to point excited harmonic load depends on the local mass, stiffness and damping. Thus by changing the thickness of a plate, crosssection of the curvilinear stiffeners and the orientation of the stiffeners we can optimize the acoustic response. Thus for a panel with two stiffeners, we have thirteen design variables  $x_1, x_2, x_3 \dots, x_{13}$  as shown in Fig. 3. The placement design variables for two stiffeners are from  $x_1$  to  $x_8$ ;  $x_9$  and  $x_{10}$  are used for height of two blade-type stiffeners;  $x_{11}$  is used for plate thickness and  $x_{12}$  and  $x_{13}$  are used to represent the thickness of two stiffeners. For a panel with six stiffeners, the design variables have increased from thirteen to

**Fig. 3** Representative thirteen design variables for a panel with two stiffeners



thirty seven as each stiffener has different thickness and height. In the design optimization framework (code named *EBF3PanelOpt* (Mulani et al. 2013) for a panel with more than two stiffeners, the placement and shape design variables for a panel with six stiffeners are from  $x_1$  to  $x_{24}$ ;  $x_{25}$  to  $x_{30}$  are used for height of six blade-type stiffeners;  $x_{31}$  to  $x_{36}$  are used for the thickness of six stiffeners and  $x_{37}$  is used to represent the thickness of the panel. The placement design variables for stiffeners can be defined in clockwise or anti-clockwise direction. The placement design variables in Fig. 3 are in clockwise direction.

#### 4.3 Objective function

There can be various possible objective functions for acoustic response of the panel with curvilinear stiffeners. The Objective function for the current work is considered to be frequency averaged radiated acoustic power, which can be obtained from the area under the radiated acoustic power versus frequency curve. Frequency averaged radiated acoustic power is defined as follows:

$$f_0 = \frac{1}{f_{span}} \int_{f_{min}}^{f_{max}} W df \quad (17)$$

Frequency is varied from  $f_{min} = 20\text{Hz}$  to  $f_{max} = 1000\text{Hz}$  with 196 increments. The  $f_{span}$  is given as the difference between  $f_{max}$  and  $f_{min}$ .

#### 4.4 Constraints

Optimizing a structure for minimum radiated acoustic power results in an increased mass of the structure. Therefore, a multi-objective design optimization problem is formulated. The mass of the structure is treated as the second objective function while constraints are placed on the buckling eigenvalue, von Mises stress and crippling stress. Table 1 shows the constraints on all the thirty seven design variables used to obtain Pareto optimal designs. The baseline design is a grid stiffened design with equal spacing between stiffeners in both the  $x$  and the  $y$  directions. Also, the stiffeners on the baseline design have a manufacturing constraint with 0.045 m as an upper bound on the height. The manufacturing constraint on the baseline design is put so that it can be manufactured by using off the shelf material (2 inch thick plate). The idea behind not having manufacturing constraint for panel with curvilinear stiffeners is to find out the potential benefit with no constraint from manufacturing (i.e. without straight stiffeners and without pre-defined size constraint).

#### 4.5 Optimizer and optimization framework

For the present optimization problem, a framework in PYTHON (code named *EBF3PanelOpt* Mulani et al. 2013) has been used. This framework provides a flexibility of using MD NASTRAN (1999) for finite element

**Table 1** Constraints on design variables

Design variable	Lower bound (m)	Upper bound (m)	Design variable	Lower bound(m)	Upper bound (m)
$x_1$	1.0668	2.1336	$x_{20}$	2.1336	3.2004
$x_2$	0.0	1.0668	$x_{21}$	0.0	1.0668
$x_3$	0.0	1.0668	$x_{22}$	0.0	1.0668
$x_4$	3.2004	4.2672	$x_{23}$	0.0	1.0668
$x_5$	1.0668	2.1336	$x_{24}$	2.1336	3.2004
$x_6$	0.0	1.0668	$x_{25}$	0.02	0.06
$x_7$	0.0	1.0668	$x_{26}$	0.02	0.06
$x_8$	3.2004	4.2672	$x_{27}$	0.02	0.06
$x_9$	1.0668	2.1336	$x_{28}$	0.02	0.06
$x_{10}$	0.0	1.0668	$x_{29}$	0.02	0.06
$x_{11}$	0.0	1.0668	$x_{30}$	0.02	0.06
$x_{12}$	3.2004	4.2672	$x_{31}$	0.002	0.006
$x_{13}$	0.0	1.0668	$x_{32}$	0.002	0.006
$x_{14}$	0.0	1.0668	$x_{33}$	0.002	0.006
$x_{15}$	0.0	1.0668	$x_{34}$	0.002	0.006
$x_{16}$	2.1336	3.2004	$x_{35}$	0.002	0.006
$x_{17}$	0.0	1.0668	$x_{36}$	0.002	0.006
$x_{18}$	0.0	1.0668	$x_{37}$	0.002	0.006
$x_{19}$	0.0	1.0668			



analysis (FEA). PYTHON scripts provide interfaces between the external optimizer and FEA as shown in Fig. 4. NSGA-II is used for multi-objective design optimization in (VisualDOC 2010) using *EBF3PanelOpt*. For NSGA-II in VisualDoc, the initial population size is chosen to be 48 and the maximum number of iterations is set to 200.

#### 4.6 Baseline grid stiffened panel design

A baseline grid stiffened panel is designed using *EBF3PanelOpt*. The baseline design optimization problem is solved for minimum mass meeting buckling, von Mises stress and crippling constraints for the loads given in Table 2. The boundary conditions and the direction of the applied loads are shown in Fig. 5. Figure 6 shows the optimized baseline grid stiffened panel. The optimized (minimum) mass for baseline grid stiffened panel is turned out to be 12.1422 kg.

### 5 Results and discussion

The role of curvilinear stiffeners to reduce the vibro-acoustic response of the stiffened panel is addressed by designing stiffened panels using developed multi-objective design optimization framework. The baseline panel is a

**Table 2** Load case for design optimization of grid stiffened baseline design

Load	(kN/m)
$N_{xx}$	11.208
$N_{yy}$	136.774
$N_{xy}$	93.693

grid stiffened panel with six stiffeners and it is obtained by performing structural (sizing) optimization for minimum mass with constraints on buckling, von Mises stress, and crippling stress. To explore the potential benefit of the curvilinear stiffeners, a multi-objective design optimization is performed where stiffeners have the freedom to have the curvilinear shape. During this multi-objective design optimization study, the mass and the radiated sound power are minimized with constraint on buckling eigenvalue, von Mises stress, and crippling stress.

The minimization of the mass and the radiated acoustic power are two objectives which conflict each other during the course of the optimization. Therefore, two Pareto optimal designs are obtained. These two Pareto optimal designs are shown in Figs. 7 and 8. The two Pareto optimal designs are chosen from a Pareto optimal front in such a way that the mass of both Pareto designs is close to the mass of the

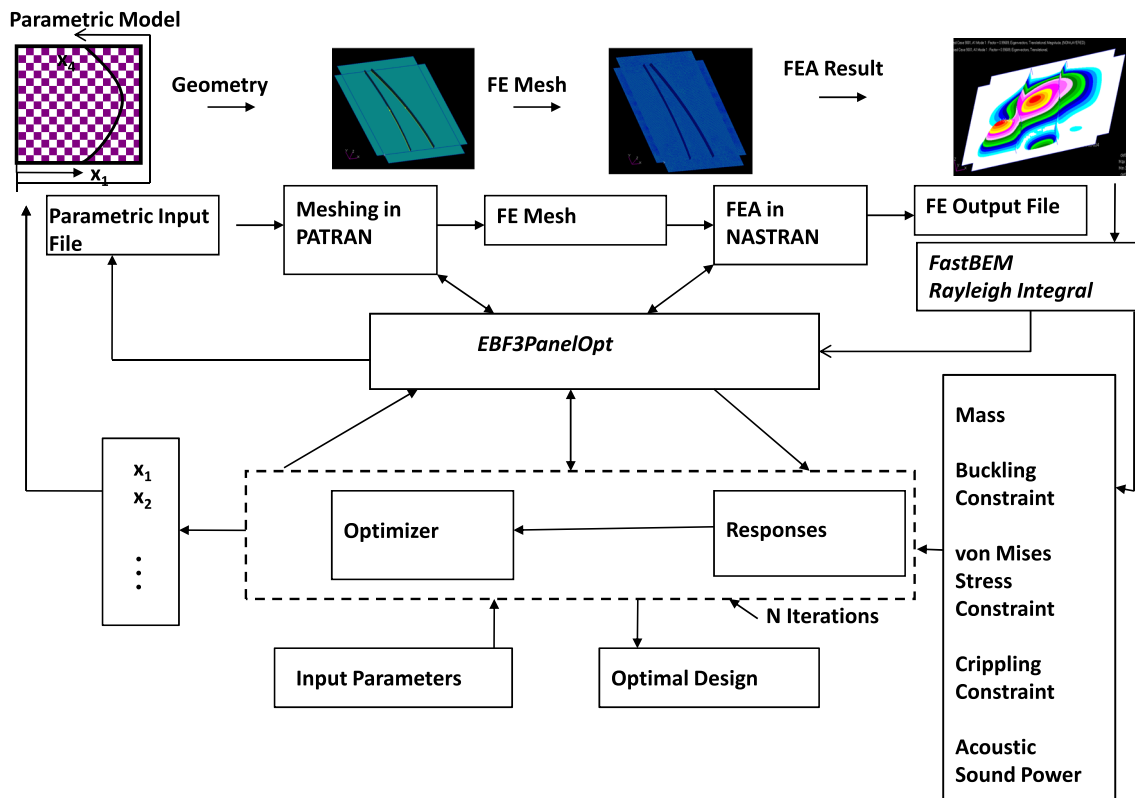


**Fig. 4** Framework for multi-objective design optimization

**Fig. 5** Simply supported boundary condition (*left*) and loads (*right*) for baseline and Pareto optimal panel design

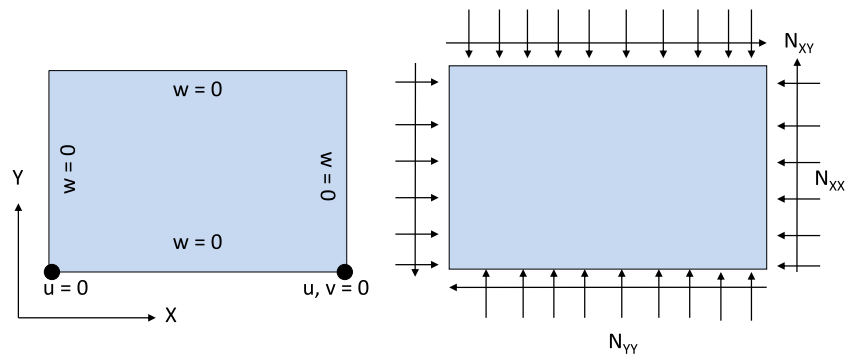


**Fig. 6** Optimal grid stiffened baseline panel with six stiffeners

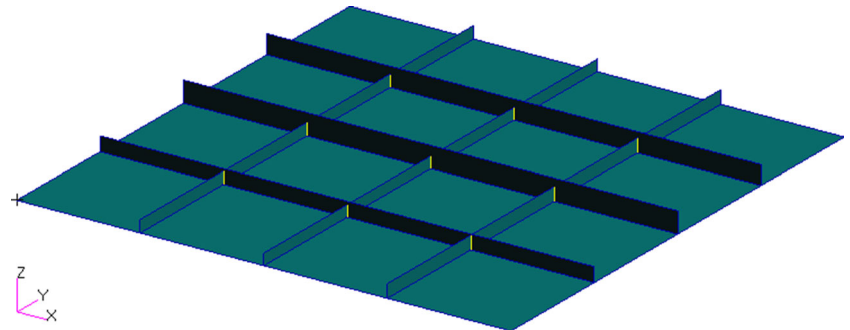


**Fig. 7** First Pareto optimal panel with curvilinear stiffeners

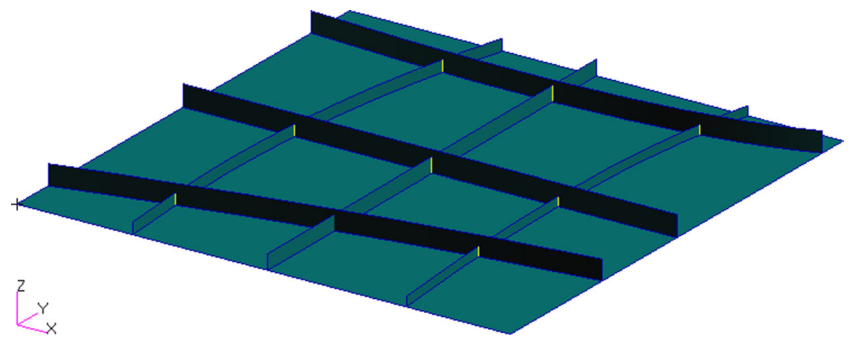


**Fig. 8** Second Pareto optimal panel with curvilinear stiffeners

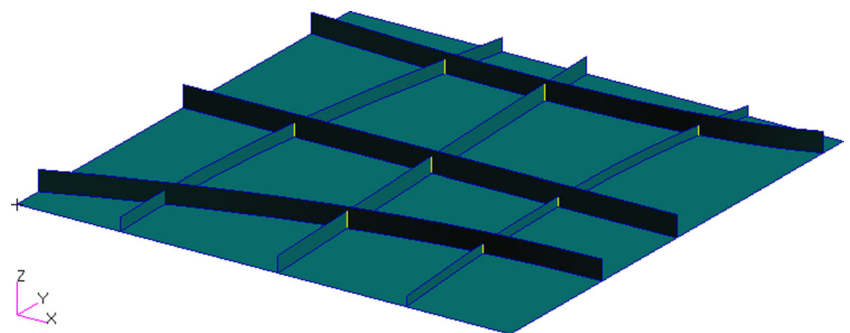




**Table 3** Numerical values of design variables for baseline and Pareto optimal designs

Design variables	Baseline design (m)	Pareto optimal design-I (m)	Pareto optimal design-II (m)	Design variables	Baseline design (m)	Pareto optimal design-I (m)	Pareto optimal design-II (m)
$x_1$	1.6000	1.6000	1.6000	$x_{20}$	2.6670	2.5453	2.6667
$x_2$	0.5000	0.5000	0.5000	$x_{21}$	0.8001	0.7271	0.8419
$x_3$	0.5000	0.5000	0.5000	$x_{22}$	0.5000	0.6333	0.6595
$x_4$	3.7338	3.7338	3.7338	$x_{23}$	0.7500	0.8598	0.7240
$x_5$	1.3335	1.1312	1.3618	$x_{24}$	2.4003	2.3702	2.3387
$x_6$	0.2500	0.1246	0.2235	$x_{25}$	0.0450	0.060	0.0455
$x_7$	0.5000	0.4323	0.5271	$x_{26}$	0.0307	0.0264	0.0424
$x_8$	4.0005	3.8271	4.1664	$x_{27}$	0.0409	0.0547	0.0429
$x_9$	1.8669	1.7575	2.0663	$x_{28}$	0.0262	0.0275	0.0251
$x_{10}$	0.7500	0.7275	0.8275	$x_{29}$	0.0243	0.0318	0.0326
$x_{11}$	0.5000	0.6470	0.6933	$x_{30}$	0.0286	0.0353	0.0202
$x_{12}$	3.4671	3.4568	3.3236	$x_{31}$	0.0040	0.0020	0.0024
$x_{13}$	0.2667	0.1840	0.2513	$x_{32}$	0.0028	0.0043	0.0024
$x_{14}$	0.5000	0.6428	0.5380	$x_{33}$	0.0020	0.0034	0.0021
$x_{15}$	0.2500	0.0828	0.1807	$x_{34}$	0.0042	0.0024	0.0022
$x_{16}$	2.9337	3.1120	2.8697	$x_{35}$	0.0020	0.0024	0.0037
$x_{17}$	0.5334	0.4090	0.5430	$x_{36}$	0.0039	0.0046	0.0020
$x_{18}$	0.5000	0.6666	0.4184	$x_{37}$	0.0034	0.0032	0.0035
$x_{19}$	0.5000	0.5085	0.5038				

baseline design. Table 3 shows the numerical values of the thirty seven design variables for baseline and Pareto optimal designs. The placement design variables in Table 3 for stiffeners are defined in anti-clockwise direction.

The radiated acoustic power versus frequency plots for the baseline grid stiffened panel and two Pareto optimal designs are compared in Fig. 9 and it is clear from this figure that most of the radiant peaks for both the Pareto optimal designs have been lowered significantly. To discuss and visualize the sound radiation property of the baseline and the two Pareto optimal designs clearly, the frequency band,

20 Hz - 1000 Hz in Fig. 9 is divided in three bands, 20 Hz - 334.9 Hz, 335 Hz - 669.9 Hz, and 670 Hz - 1000 Hz, respectively. Radiated acoustic power of the baseline and Pareto optimal designs for these three different bands is compared in Figs. 10, 11 and 12, respectively. It is clear from Fig. 10 that both Pareto optimal designs perform better than the baseline design in the band, 20 Hz - 334.9 Hz. In this band, both Pareto optimal designs have reduced the height of the most radiant peak (first) of the baseline design significantly.

In the whole frequency band of interest, 20 Hz - 1000 Hz, the most significant contribution is from the first band.

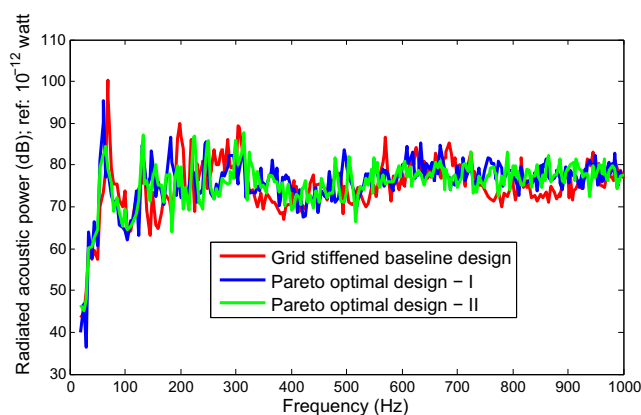


**Fig. 9** Comparison of radiated acoustic power of baseline and two Pareto optimal designs for a band from 20 Hz to 1000 Hz

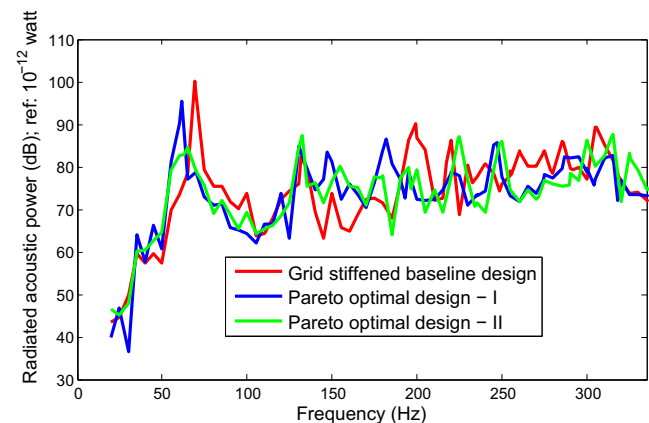


**Fig. 10** Comparison of radiated acoustic power of baseline and two Pareto optimal designs for a band from 20 Hz to 334.9 Hz

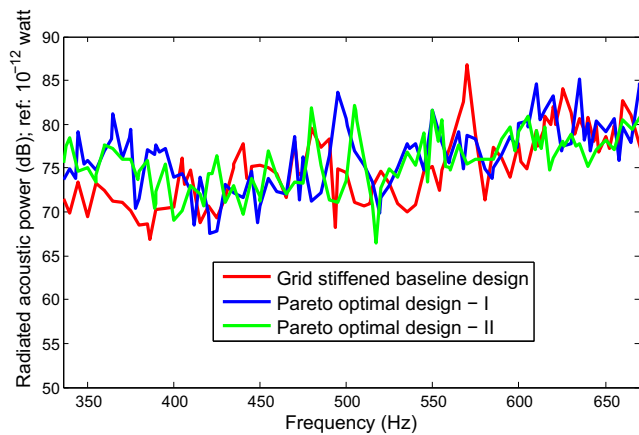


**Fig. 11** Comparison of radiated acoustic power of baseline and two Pareto optimal designs for a band from 335 Hz to 669.9 Hz

Therefore, the radiated acoustic power of the baseline and the Pareto optimal designs at the natural frequencies corresponding to first three mode shapes is presented in Table 4. It is clear from this Table that the most radiant peak of first Pareto optimal design (95.5 dB) is reduced by 4.7 dB when compared to the most radiant peak of the baseline design. Similarly, the most radiant peak of second Pareto optimal design (87.3 dB) is reduced by 12.9 dB when compared to the most radiant peak of the baseline design. The contour plot of vibrational velocity (magnitude of velocity) due to diffuse field excitation can be used to justify this huge reduction in sound radiation at the natural frequencies corresponding to first three modes of all three designs. Therefore, Fig. 13 shows the contour plot of velocity response (magnitude) of the baseline and the Pareto optimal designs at the natural frequencies corresponding to first three modes of these designs to diffuse field excitation.

From Fig. 13, it can be seen that the scale (maximum) for velocity contour of the first Pareto optimal design at the

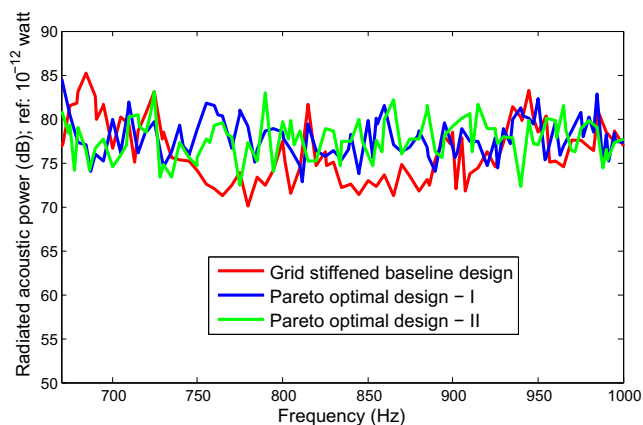


**Fig. 12** Comparison of radiated acoustic power of baseline and two Pareto optimal designs for a band from 670 Hz to 1000 Hz

**Table 4** Radiated acoustic power at natural frequencies corresponding to first three mode

Mode number	Radiated acoustic power (dB) Baseline design	Radiated acoustic power (dB) Pareto optimal design-I	Radiated acoustic power (dB) Pareto optimal design-II
1	100.2	95.5	82.9
2	82.2	84.8	87.3
3	90.0	83.5	80.0

Shapes of grid stiffened baseline design, Pareto optimal design-I and Pareto optimal design-II

natural frequency corresponding to first mode has reduced to 0.0186 m/s (35.6 % reduction when compared to the baseline). For the second Pareto optimal design, the scale (maximum) for velocity contour at the natural frequency corresponding to first mode has reduced to 0.00422 m/s (85.4 % reduction when compared to the baseline). In Fig. 13 the velocity response of Pareto optimal designs at natural frequencies corresponding to second and third mode shapes have transformed one of the two lobes of the baseline design with high velocity response into a lobe of Pareto optimal design with lower velocity response thus making the Pareto optimal designs quieter with reduced sound radiation capability.

From Fig. 11, it can be seen that the most radiant peak in the second band, 335 Hz - 669.9 Hz, is of the baseline design and the peaks of the Pareto optimal designs are significantly lower than the most radiant peak of the baseline design. Similarly, the most radiant peak in the third band is of the baseline design and the most radiant peak of the Pareto optimal designs are approximately 1 dB lower than the most radiant peak of the baseline design in the third band. Overall, both the frequency-averaged radiated acoustic power in the band, 20 Hz - 1000 Hz, and the mass for the first Pareto optimal design is reduced when compared to the baseline design. The Pareto optimal designs have significant reduction in frequency-averaged radiated acoustic power when compared to the baseline design. The mass of the second Pareto optimal design is 0.35 % (0.0422 kg) higher than the mass of the baseline design. In summary, the second Pareto optimal design is the best Pareto optimal design as it has reduced the frequency-averaged radiated acoustic power by 2.3 dB without increasing the mass significantly (0.35 % higher than the baseline design).

From Table 5, it is to be noticed that all three designs satisfy the buckling, von Mises stress and crippling constraints. It is to be noted that the tolerance for constraint violation in optimizer (VisualDoc) is set to a default value of 0.003. Due to this tolerance, the value of the buckling factor of the

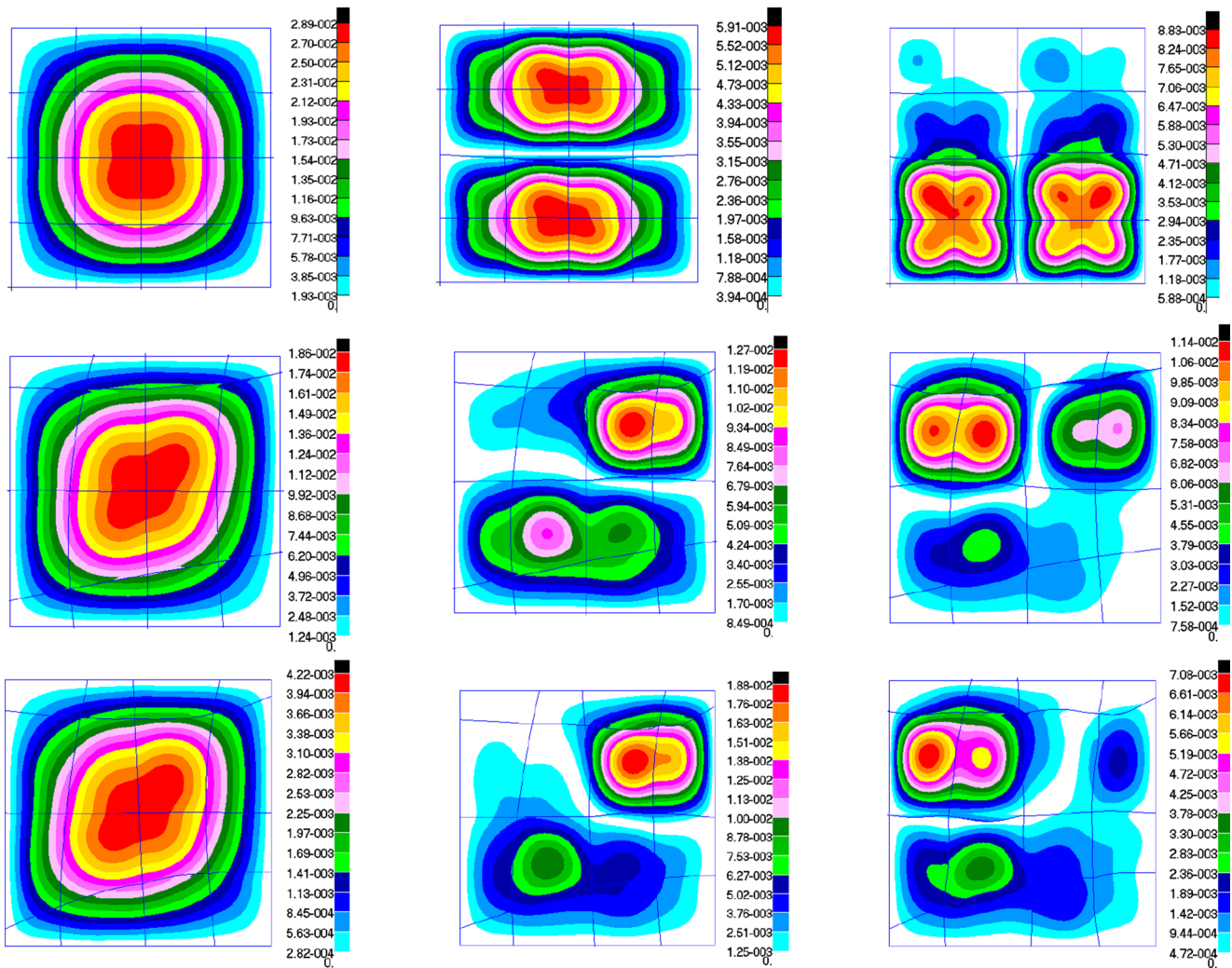


**Fig. 13** Contour of velocity (magnitude) response at first three natural frequencies of grid stiffened baseline design (*top row*), Pareto optimal design-I (*middle row*) and Pareto optimal design-II (*bottom row*)

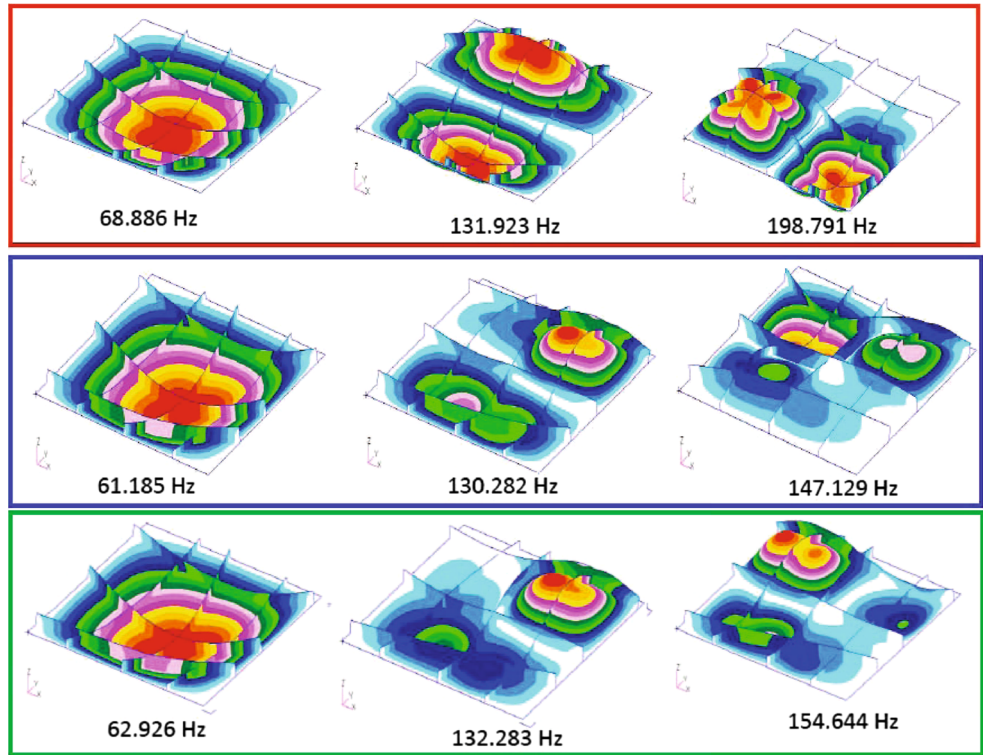
baseline design (as shown in Table 5) is 1.003 and is considered not to be violated. The first nine mode shapes of the baseline and the two Pareto optimal designs are shown in Figs. 14, 15, and 16, respectively. It is clear from these figures that curvilinear stiffeners are changing the radiant mode of the baseline panel into a relatively quieter mode of the Pareto optimal designs in the band of interest (20 Hz-

1000 Hz). This phenomena is occurring due to the freedom for placement and curvature of the stiffeners in the Pareto optimal design as opposed to the grid stiffened design where the placement and curvature is fixed. From Figs 15–16 it is seen that the curvilinear stiffener designs (Pareto optimal designs) have less number of excited lobes than the baseline design. At a particular frequency, the lesser number of

**Table 5** Comparison of optimal designs

Panel	Frequency averaged radiated acousticpower (dB)	Mass (kg)	Buckling factor	von Mises stress constraint	Crippling stress constraint
Baseline	80.3	12.1422	1.003	0.1289	0.1932
Pareto optimal-I	78.8	12.1297	0.995	0.1259	0.191
Pareto optimal-II	78.0	12.1842	0.991	0.126	0.2127

**Fig. 14** First, second and third mode shapes and corresponding natural frequencies for grid stiffened baseline design (top  ), Pareto optimal design-I (middle  ), and Pareto optimal design-II (bottom  )



distinct lobes will displace the smaller acoustic medium thus radiating less in the medium adjacent to the structure.

The CPU time for all the optimization studies performed in this manuscript is not quantified. However, it

is worth mentioning that the qualitative time for baseline design is approximately one day and for the multi-objective design optimization task, it is approximately five days.

**Fig. 15** Fourth, fifth and sixth mode shapes and corresponding natural frequencies for grid stiffened baseline design (top  ), Pareto optimal design-I (middle  ), and Pareto optimal design-II (bottom  )

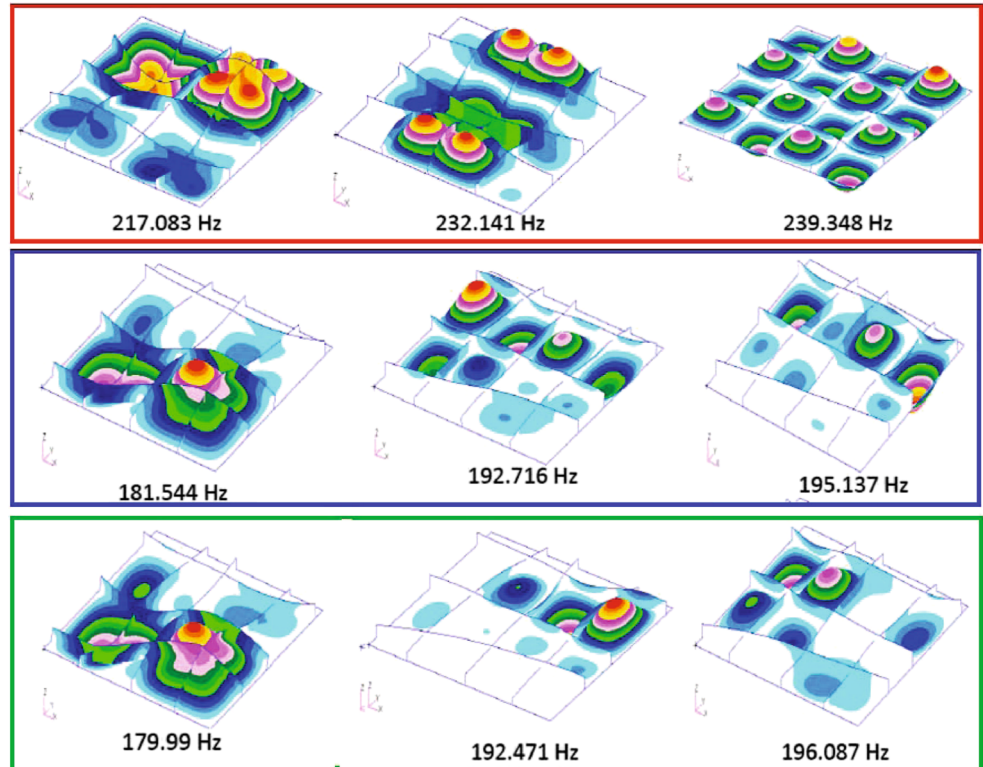
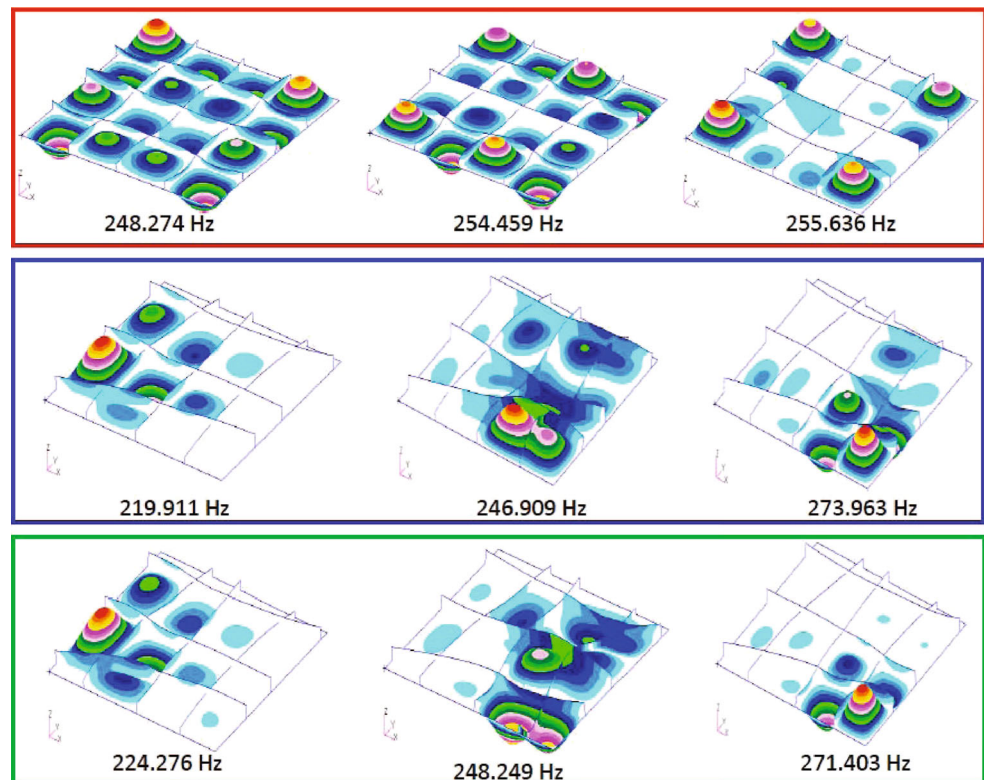




**Fig. 16** Seventh, eighth and ninth mode shapes and corresponding natural frequencies for grid stiffened baseline design (top □), Pareto optimal design-I (middle □), and Pareto optimal design-II (bottom □)



## 6 Conclusion and future work

A multi-objective design optimization study is performed for a panel with six stiffeners. It is concluded from this study that the panel with curvilinear stiffeners play an important role in breaking the radiant mode of the stiffened panel as the curvilinear stiffeners have freedom to move in the design domain and perform better than a grid stiffened design of almost equivalent mass. As far as the future work is concerned, the constraint of having three stiffeners along the length and the other three stiffeners along the width of the panel will be relaxed and the whole design space will be explored for the placement optimization of six stiffeners. The present capability of the framework will also be extended to perform multi-objective design optimization of curved panel with straight and curvilinear stiffeners under diffuse field excitation.

**Acknowledgments** The work presented here is funded under NASA Subsonic Fixed Wing Hybrid Body Technologies NRA (NASA NN L08AA02C) with Ms. Karen Taminger as the Program Manager (PM) and Mr. Keith Bird as Contracting Officer's Technical Representative (COTR). We are thankful to both Ms. Taminger and Mr. Bird for their suggestions. The authors would like to thank Mr. Dan Palumbo and the *EBF3* team at NASA Langley Research Center for technical discussions. The authors would also like to thank our partners in the NRA project, Mr. Bob Olliffe, Mr. David Havens and Dr. Steve Englestadt all of Lockheed Martin Aeronautics Company of Marietta, GA, for technical discussions.

## References

- Graham WR (1996) Boundary layer induced noise in aircraft, Part I: The flat plate model. *J Sound Vib* 192(1):101–120
- Graham WR (1996) Boundary layer induced noise in aircraft, Part II: The trimmed flat plate model. *J Sound Vib* 192(1):121–138
- Koopmann GH, Fahline JB (1997) *Designing Quiet Structures: A Sound Power Minimization Approach*. Academic Press, San Diego
- Denli H, Frangakis S, Sun JQ (2005) Normalization in acoustic optimization with rayleigh integral. *J Sound Vib* 284:1229–1238
- Jeon JY, Okuma M (2004) Acoustic radiation optimization using the particle swarm optimization algorithm. *JSME Int J Series C* 47(2):560–567
- Belegundu AD, Salagame RR, Koopmann GH (1994) A General optimization strategy for sound power minimization. *Struct Multidiscip Optim* 8:113–119
- Lu-yun C, De-yu W (2007) Structural-acoustic optimization of stiffened panels based on a genetic algorithm. *J Mar Sci Appl* 6(4):55–61
- Fourie PC, Groenwold AA (2002) The particle swarm optimization algorithm in size and shape optimization. *Struct Multidiscip Optim* 23:259–267
- St. Pierre RL, Koopmann GH (1993) Minimization of Radiated Sound Power From Plates Using Distributed Point Masses, presented at the ASME Winter Annual Meeting, New Orleans, LA, November 28 - December 3, 1993, Paper no. 93-WA/NCA-11
- Cunefare KA (1990) *The Design Sensitivity and Control of Acoustic Power Radiation by Three-dimensional Structures*, PhD Dissertation. The Pennsylvania State University, Pennsylvania
- Naghshineh K, Koopmann G, Belegundu A (1992) Material tailoring of structures to achieve a minimum radiation condition. *J Acoust Soc Am* 92(2,Pt.1):841–855

- Pierce AD (1989) *Acoustics: An Introduction to its Physical Principles and Applications*, Acoustical Society of America, New York, 1989, pp 159–166
- Hekamati A, Ricot D, Druault P (2010) Vibroacoustic Behavior of a Plate Excited by Synthesized Aeroacoustic Pressure Fields, AIAA 2010-3950, 16<sup>th</sup> AIAA/CEAS Aeroacoustics Conference, 7-9 June 2010, Stockholm, Sweden
- Maury C, Gardonio P, Elliott SJ (2002) A wavenumber approach to modelling the response of a randomly excited panel, Part I: General Theory. *J Sound Vib* 252(1):83–113
- Joshi P, Mulani SB, Gurav SP, Kapania RK (2010a) Design optimization for minimum sound radiation from point-excited curvilinearly stiffened panel. *J Aircr* 47(4):1100–1110. doi:[10.2514/1.44778](https://doi.org/10.2514/1.44778)
- Joshi P, Mulani SB, Kapania RK, Slemp WCH (2010b) Minimization of Acoustic Radiation from a Turbulent Boundary Layer Excited Panel with Curvilinear Stiffeners, AIAA 2010-2541, 51<sup>st</sup> AIAA/ASME/ASCE/AHS/ASC Structures, Structural Dynamics, and Materials Conference, 12–15 April 2010, Orlando, Florida
- Faust M, Piret G (1996) Vibro-acoustic Payload Effect Tests of the Ariane 5 Fairing with Olympus Satellite in ESTEC-LEAF, Proceedings of the Conference on Spacecraft Structures, Materials and Mechanical Testing, 27–29 March 1996, Noordwijk, Netherlands
- Buehrle RD, Gibbs GP, Klos J, Mazur M (2003) Modelling and Validation of Damped Plexiglass Windows for Noise Control, AIAA 2003-1870, 44<sup>th</sup> AIAA/ASME/ASCE/AHS Structures, Structural Dynamics, and Materials Conference, 7–10 April 2003, Norfolk, Virginia
- Deb K, Pratap A, Agarwal S, Meyarivan T (2002) A fast and elitist multiobjective genetic algorithm: NSGA-II. *IEEE Trans Evol Comput* 6:2
- Mulani SB, Slemp WCH, Kapania RK (2013) EBF3PanelOpt: an optimization framework for curvilinear blade-stiffened panels. *Thin-Walled Struct* 63:13–26
- Rafaely B (2000) Spatial-temporal correlation of a diffuse sound field. *J Acoust Soc Am* 107(6):3254–3258
- Constans EW, Belegundu AD, Koopman GH (1998) Design approach for minimizing sound power from vibrating shell structures. *AIAA J* 36(2):134–139
- MD. NASTRAN R2.1 (1999) MSC Software Corporation, Santa Ana, California, USA
- Wallace CE (1972) Radiation resistance of a rectangular panel. *J Acoust Soc Am* 51:946–952
- Fahy F. (1985) *Sound and structural vibration*. Academic Press, New York
- VisualDOC 6.2.2 (2010) Vanderplaats Research and Development, Inc. Colorado Springs, CO 80906, USA